J. Biochem. **144,** 675–684 (2008)
doi:10.1093/jb/mvn116

Role of the Aromatic Residues in the Near-amino Terminal Motif of Vimentin in Intermediate Filament Assembly *In Vitro*

Rumi Gohara[1], Sadakatsu Nishikawa[2], Yozo Takasaki[1] and Shoji Ando[1,*]

[1]Division of Biopolymer Research, Department of Biomolecular Sciences, Faculty of Medicine, Saga University, Saga 849-8501; and [2]Department of Applied Chemistry, Faculty of Science and Engineering, Saga University, Saga 840-8502, Japan

Received August 18, 2008; accepted September 6, 2008; published online September 19, 2008

Type III and IV intermediate filament (IF) proteins share a conserved sequence motif of -Tyr-Arg-Arg-X-Phe- at the near-amino termini. To characterize significance of the aromatic residues in the motif, we prepared vimentin mutants in which Tyr-10 and Phe-14 are substituted with Asn and Ser (Vim[Y10N], Vim[F14S] and Vim[Y10N, F14S]), and examined assembly properties *in vitro* by electron microscopy and viscosity measurements. At 2 s after initiation of assembly reaction at pH 7.2 and 150 mM NaCl, all the vimentin mutants formed so-called unit-length filaments (ULFs) that were slightly larger than ULFs of wild-type vimentin. In following filament elongation, Vim[Y10N, F14S] and Vim[Y10N] performed longitudinal annealing of ULFs very rapidly and formed IFs within only 2.5 and 5 min, respectively, while Vim[F14S] and wild-type vimentin gave IFs by 40–60 min. The IFs of Vim[Y10N, F14S] and Vim[Y10N], however, tended to intertwine each other and formed bundles in parts of the specimens. The intertwinements decreased as the salt concentration decreased, and optimal salt concentration for the two mutants to form normal IFs was 50 mM. These results suggest that the aromatic residues, especially Tyr-10, in the motif have a role in controlling intermolecular interactions involved in IF assembly *in vitro* and suppress undesirable filament intertwinements at physiological ionic strength.

Key words: electron microscopy, intermediate filament, site-directed mutagenesis, vimentin, viscosity.

Abbreviations: EM, electron microscopy; IF, intermediate filament; MES, 2-(*N*-morpholino)ethanesulphonic acid; PCR, DNA polymerase chain reaction; PMSF, phenylmethylsulphonyl fluoride; ULF, unit-length filament.

Intermediate filaments (IFs) are major components of the cytoskeleton and the nuclear lamina of most eukaryotic cells (*1–6*). A major function of IFs is to contribute the maintenance of cellular integrity in the presence of mechanical stress, and mutations in human IF genes have been related to a variety of tissue-specific disorders (*1*, *4*, *7*). IFs are comprised of a large family of gene products (~70 members for humans) that are capable of polymerized into 10 nm diameter filaments (*8*). From the extent of sequence homology and the pattern of cell-type-specific expression, IF subunit proteins are classified into at least five different types: acidic keratins of epithelia are type I; neutral–basic keratins of epithelia are type II; vimentin present primarily in mesenchymal cells, desmin of most muscles and glial fibrillary acidic protein of astroglia are type III; the three neurofilament proteins, nestin and α-internexin of the nervous system are type IV; lamins of nuclear lamina are type V. All IF subunit proteins share a characteristic tripartite structure that includes the central α-helical rod domain flanked by the non-α-helical N-terminal head and C-terminal tail domains (*1*, *4–6*). The rod domain, consisting of approximately 310 amino acids (for lamins 350 amino acids), has relatively conserved sequences at the N- and C-terminal ends, and displays long heptad-repeat patterns (*abcdefg*) of hydrophobic residues (*a* and *d*). The heptad-repeat patterns are interrupted in several places, and resultantly the rod domain can be further subdivided into four helices 1A, 1B, 2A and 2B. In contrast, the head and tail domains have variable length, sequences and chemical characteristics among IF protein types.

The IF subunit proteins readily associate into a coiled-coil dimer in a parallel in-register manner (*1*, *4–6*). The rod domain is responsible for the dimer formation. Two dimers associate into a tetramer, in an anti-parallel and a half-length staggered manner, resulting 65 nm long particles with a diameter of 2.5 nm. It was suggested that the homotypic interactions between neighbouring coiled-coil helices 1B of two dimers (*i.e.* A_{11} alignment) or between coiled-coil helices 2B of two dimmers (A_{22} alignment) are responsible for the tetramer formation (*1*, *4–6*, *9–13*). Another type of alignment, A_{12}, in which two dimmers are anti-parallel and fully overlapped, is not found at the tetrameric stage, but only at hexameric, octameric or higher oligomeric stages, while tetramer in this alignment is only stable at high pH values which does not permit IF formation (*4*, *10*, *13*). Tetramers have indeed been demonstrated to exist, albeit in small amounts, in living cells (*3*).

*To whom correspondence should be addressed. Tel: +81-952-34-2192, Fax: +81-952-34-2418, E-mail: andohs@cc.saga-u.ac.jp

Molecular mechanisms for higher assembly steps from tetramers into IFs are not well understood (*1*, *4–6*). Concerning the assembly *in vitro* of cytoplasmic IF proteins, Ip *et al*. (*14*) have demonstrated by electron microscopy that, under certain ionic and pH conditions, vimentin tetramers associate into short filaments with a full-width (10–12 nm) and a length of ~66 nm, and that the short filaments elongate into IFs. Herrmann *et al*. have examined extensively IF formation by electron microscopy and reported that, under a physiological solution condition, tetramers of vimentin, desmin or keratins associate laterally to form a unit-length filament (ULF) with a full-width (~16 nm) and a length of ~60 nm, consisting of most typically eight tetramers (*15–18*). Then ULFs anneal longitudinally into filaments with several hundred nanometres long, and finally the filaments undergo a cooperative radial compaction to form mature IFs with a diameter of ~10 nm (*15–18*). We have analysed the assembly intermediates *in vitro* of vimentin by atomic force microscopy and showed that a ULF of 60–70 nm long has four segments with a convex surface and that the longitudinal annealing of ULFs proceeds with an elongation step of ~40 nm, suggesting that the annealing occurs by overlapping two segments of each ULF (*19*).

Importance of the central rod domain as the basic IF construction element is reflected by the strong, negative influence of point mutations in the highly conserved end regions of this domain on the IF assembly competence *in vitro* and *in vivo* (*1*, *4*, *5*, *20–22*). The tail domain is largely dispensable for IF assembly, since proteolytic removal or genetically engineered deletion of the tail domain does not prevent IF formation (*1*, *4*, *15*), although the tail domain might play a subtle role in filament formation or stability. In contrast, the head domain is apparently crucial for IF assembly. IF proteins lacking the head domain by limited proteolysis or genetic engineering are assembly incompetent *in vitro* and *in vivo*, and remain dimers and tetramers in an IF assembly condition (*1*, *4*, *5*, *15*, *23–25*). Stepwise deletion from the N-terminus of the head domain of desmin and vimentin suggested that a short sequence motif -Tyr-Arg-Arg-X-Phe-, which is localized at the beginning of the head domain and shared by most of the type III and type IV IF proteins, is important for IF assembly *in vitro* and *in vivo*, although this motif alone is not sufficient for normal IF assembly (*21*, *25–29*). These results were confirmed and extended by arginine point mutations in this motif, which showed that only one of the two adjacent arginine residues is essential for IF assembly of vimentin and desmin (*21*, *26*, *29*). On the other hand, significance of the aromatic residues preceding or following the arginine residues has remained to be determined. In order to characterize the role of each aromatic residue in the motif, we prepared recombinant mouse vimentin mutants in which Tyr-10 and Phe-14 are substituted with Asn and Ser, and examined their assembly properties *in vitro* by electron microscopy and viscosity measurements. We observed that the substitution of the aromatic residues, especially Tyr-10, unexpectedly accelerate the longitudinal annealing of ULFs into IFs and causes filament intertwinements at physiological ionic strength.

MATERIALS AND METHODS

Site-directed Mutagenesis and Construction of Expression Vectors—Full-length murine vimentin cDNA (1.4 kb) flanked by *Nde*I and *Bam*HI restriction sites (*30*) was used as the starting material for all plasmid construction. Site-directed mutagenesis was performed by oligonucleotide-directed dual amber method, using Mutan-Super Express Km site-directed mutagenesis kit with pKF18k vector (Takara, Kusatsu, Japan) as follows. The vimentin cDNA was subcloned into an *Nde*I–*Bam*HI digested pKF18k-2 plasmid. LA(long and accurate)-PCR was performed using an oligonucleotide primer that contains the desired mutation and the selection primer that reverts the amber mutations on the kanamycin-resistant gene in the plasmid. The primer sequences used for mutation were as follow: 5′-TCGTCCTCCAACCGCAGGATG-3′ for Vim[Y10N]; 5′-CAGGATGTCCGGTGGCTCC-3′ for Vim[F14S]; 5′-TCCTCCTACAGCAGTATGTTC-3′ for Vim[R11S, R12S]. The PCR products were transformed into *Escherichia coli* MV1184, and then the transformants containing the desired mutation were grown on the medium containing kanamycin. For the double mutations of Vim[Y10N, F14S], the Vim[Y10N] DNA fragment was excised with *Nde*I and *Bam*HI, subcloned again into pKF18k-2 plasmid, and then applied to the second LA-PCR using the primers for the F14S mutation and kanamycin-resistant selection. Clones were picked at random, and the identity of mutations was verified by DNA sequencing. The inserts were excised with *Nde*I and *Bam*HI, and subcloned into *Nde*I–*Bam*HI-digested pET-3a vectors (Novagene, Madison, USA) for bacterial expression.

Bacterial Expression and Protein Purification—Each plasmid was transformed into *E. coli* BL21(DE3)pLysS (Novagene). The cells were cultured overnight in LB medium containing chloramphenicol (34 μg/ml) and ampicillin (100 μg/ml), diluted 1 : 100 with the fresh LB medium, and grown to an OD_{600} of 0.6. Isopropyl-1-thio-β-D-galactopyranoside was then added to a final concentration of 0.4 mM to induce expression. After shaking at 37°C for 3 h, the cells were harvested by centrifugation and sonicated in 10 mM Tris–HCl pH 7.5, 10 mM EDTA, 10 mM β-mercaptoethanol, 1 mM PMSF, 300 mM KCl (buffer A). The homogenate was centrifuged at 25,000*g* at 4°C for 1 h, and the resulting pellet was washed with buffer A containing 0.5% Triton X-100, then dissolved in 10 mM Tris–HCl pH 7.5, 2 mM EDTA, 10 mM β-mercaptoethanol, 1mM PMSF, 8 M urea (buffer B). After centrifugation at 100,000*g* at 4°C for 1 h, the supernatant was applied to a Q-Sepharose column (1.6 × 5 cm) equilibrated with 10 mM Tris–HCl pH 7.5, 1 mM EDTA, 10 mM β-mercaptoethanol, 0.5 mM PMSF, 6 M urea (buffer C). Proteins were eluted from the column by application of a linear concentration gradient of NaCl (0–0.6 M) in buffer C. The fractions containing desired proteins were pooled and dialysed against 20 mM MES–NaOH pH 6.0, 1 mM EDTA, 10 mM β-mercaptoethanol, 0.5 mM PMSF, 6 M urea (buffer D) and then applied to a SP-Sepharose column (1.6 × 5 cm) equilibrated with the same buffer. Proteins were eluted from the column by application of a linear concentration gradient of NaCl (0–0.6 M) in buffer D. The fractions

containing desired proteins were collected, dialysed against 10 mM Tris–HCl pH 9.0, 2 mM EDTA, 10 mM β-mercaptoethanol (buffer E), cleared of aggregates by centrifugation at 100,000*g* at 4°C for 1 h, and stored at −20°C. The authenticity of proteins was verified by SDS–polyacrylamide gel electrophoresis and amino terminal sequence analysis using a Shimadzu PPSQ system. First methionine residue of the initiation codon was found to be removed in the expression system used here, and the amino terminal sequences started with a serine residue, as shown in Fig. 1. Concentrations of proteins were determined by the method of Bradford (*31*), using bovine serum albumin as a standard.

In Vitro *Filament Assembly*—IF assembly was carried out in 20 mM imidazole–HCl pH 7.2, 50–150 mM NaCl, 2 mM β-mercaptoethanol (assembly buffer) at 37°C. Protein concentration was adjusted to 0.2 mg/ml. The IF assembly reaction was initiated by addition of the soluble protein (1.0 mg/ml) in buffer E to four volumes of the concentrated assembly buffer (25 mM imidazole–HCl pH 7.0, 62.5, 125 or 187.5 mM NaCl) and then rapid mixing (dilution method). At various time points, 20 μl of the reaction mixture was withdrawn and added to 20 μl of the assembly buffer containing 0.2% glutaraldehyde. Glutaraldehyde was used to stop the assembly reaction and to fix the products by cross-linking (*15*, *19*, *32*). After 5 min of fixation at room temperature, the final 20 μl was served for electron microscopic analysis.

Electron Microscopy—IF preparations were placed directly on carbon film-coated specimen grids, stained with 2% uranyl acetate, and analysed using a JEM-1210 electron microscope (JEOL, Tokyo, Japan) that was operated at an accelerating voltage of 80 kV.

Viscosity Measurements—An Ostwald viscometer (Moritomo Rika, Osaka, Japan) with a sample volume of 1.2 ml and buffer flow time of 21 s at 30°C was used in a water bath with a temperature control device. The U-shaped viscometer includes a section with a narrow diameter through which the sample flows driven by hydrostatic pressure. The time required for the solution to pass through an upper and lower mark of the glass capillary tube was recorded. IF assembly was carried out at 30°C in the assembly buffer containing 0.005% Tween-20 and 1 mM DTT instead of β-mercaptoethanol. Protein concentration was adjusted to 0.3 mg/ml. After initiation of the IF assembly reaction by addition of the soluble protein in buffer E to the concentrated assembly buffer and rapid mixing, the sample was immediately introduced into the viscometer, and then viscosity was measured at regular, specified intervals. Specific viscosity (η_{sp}) is calculated by the equation

$$\eta_{sp} = (t_s - t_b)/t_b$$

where, t_s is the flow time of the sample and t_b is the flow time of the assembly buffer only.

Curves representing the time course of viscosity increase were fitted by cubic equations. Initial rate in the increase of viscosity was estimated by differential of the equation at time zero second.

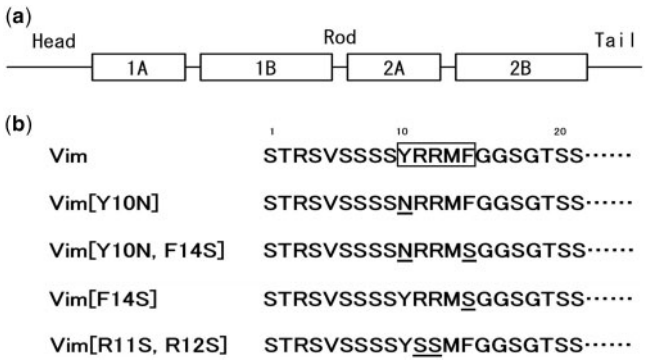

Fig. 1. **Schematic presentation of the domain structure of mouse vimentin (a) and amino acid sequences of vimentin mutant proteins (b)**. In (a), the boxes represent the helices 1A, 1B, 2A, and 2B of the central α-helical rod domain, the lines the non-α-helical head and tail domains, as well as the non-α-helical spacer sequences. In (b), the conserved motif is boxed. The amino acid substitutions in the motif are underlined.

RESULTS

Preparation of Vimentin Mutants—The structures of mouse vimentin mutants prepared in this study are schematically shown in Fig. 1. To examine significance of the aromatic residues in the sequence of -Tyr-Arg-Arg-Met-Phe-, Tyr-10 and Phe-14 were substituted with Asn and Ser, respectively. The abbreviated names of the vimentin mutants (Vim[Y10N], Vim[Y10N, F14S] and Vim[F14S]) indicate the substituted amino acid residues in single-letter codes, their positions, and newly introduced amino acids, in the angle brackets. These site-directed mutations were introduced into the mouse vimentin cDNA, by PCR using oligonucleotide primers that contain the desired mutation, as described under MATERIALS AND METHODS section. In addition, mutation that replaces both Arg-11 and Arg-12 with Ser was also introduced, to obtain an IF assembly-incompetent vimentin mutant (*21*, *26*, *29*). The recombinant proteins were bacterially expressed and purified from inclusion bodies by ion-exchange column chromatography using 6 M urea, as described under MATERIALS AND METHODS section. After dialysis against a buffer of pH 9, these proteins were obtained as soluble oligomers.

The assembly reaction was initiated by transferring the soluble proteins to a standard assembly buffer of pH 7.2 with physiological ionic strength (150 mM NaCl), and then rapid mixing. Since ionic strength affects IF formation and stability, the experiments were also carried out at 100 or 50 mM NaCl. Protein concentration in the assembly reaction mixture was adjusted to 0.2 mg/ml. At various time points, an aliquot of the reaction mixture was withdrawn, treated with 0.1% glutaraldehyde to stop the assembly reaction (*15*, *19*, *32*), and then served for electron microscopic analysis, as described under MATERIALS AND METHODS section.

Effects of Substitution at Tyr-10 and Phe-14 on ULF Formation—At 2 s after initiation of the assembly reaction at 150 mM NaCl, wild-type vimentin formed short full-width filaments, called ULFs, with a length of 62 ± 7 nm and a width of 16 ± 2 nm (Fig. 2a) (*15*, *18*, *19*). All the mutant proteins prepared here also afforded ULFs. Vim[Y10N] formed ULFs with a length of 70 ± 7 nm

and a width of 23 ± 3 nm (Fig. 2b), Vim[Y10N, F14S] formed ULFs with a length of 67 ± 9 nm and a width of 23 ± 4 nm (Fig. 2c), and Vim[F14S] formed ULFs with a length of 60 ± 7 nm and a width of 19 ± 2 nm (Fig. 2d). Thus, substitution of the aromatic residues, especially Tyr-10, in the near-amino terminal motif resulted in formation of ULFs that appeared to be larger than those of wild-type vimentin at 150 mM NaCl. Similar results were also obtained at 100 mM NaCl (data not shown). The ULFs of the mutant proteins with increased widths might be composed of a larger number of tetramers per cross-section than the number of wild-type vimentin tetramers, although the exact numbers were not determined. These results suggest that substitution of the aromatic residues in the motif enhanced the lateral association of vimentin tetramers to form relatively thick ULFs. In addition, the relatively longer ULFs compared to those of wild-type vimentin suggest that longitudinal filament elongation had already started for Vim[Y10N] and Vim[Y10N, F14S].

At 50 mM NaCl, the sizes of the ULFs of Vim[Y10N] and Vim[Y10N, F14S] were closed to those of wild-type vimentin ULFs: wild-type vimentin formed ULFs with a length of 58 ± 7 nm and a width of 18 ± 2 nm (Fig. 2f), Vim[Y10N] formed ULFs with a length of 57 ± 5 nm and a width of 17 ± 2 nm (Fig. 2g), Vim[Y10N, F14S] formed ULFs with a length of 57 ± 5 nm and a width of 16 ± 2 nm (Fig. 2h), and Vim[F14S] formed ULFs with a length of 58 ± 7 nm and a width of 17 ± 2 nm (Fig. 2i). Thus, an apparent effect of substitution at Tyr-10 and Phe-14 on ULF formation was not observed at 50 mM NaCl. Interestingly, decrease of the salt concentration from 150 to 50 mM significantly reduced the sizes of ULFs of Vim[Y10N] and Vim[Y10N, F14S]. These results suggest that in ULF formation the lateral association of tetramers of the mutant proteins significantly depends on ionic strength.

Vim[R11S, R12S] did not form ULFs but gave mainly globular aggregates at 50–150 mM NaCl (Fig. 2e and j), although small amounts of ULF-like structures were barely seen at 50 mM NaCl (Fig. 2j, left side). Thus, substitution of both the arginines severely affected ULF formation, suggesting that the two arginines in the near-amino terminal motif are critically involved in ULF formation. In contrast, Tyr-10 and Phe-14 appeared to control lateral association of tetramers in ULF formation, depending upon ionic strength employed in the assembly reaction.

Effects of Substitution at Tyr-10 and Phe-14 on Filament Elongation—In the next step, ULFs anneal longitudinally into longer assembly intermediates (*15*, *18*, *19*). At 150 mM NaCl, wild-type vimentin gave assembly intermediates with lengths of 150–300 nm at 2.5 min (Fig. 3a), then formed those with lengths of several hundreds nanometers at 10 min (Fig. 3b). The widths of these assembly intermediates were ~16 nm, almost the same with the width of ULFs. Until 10 min, ULFs had been almost consumed for filament elongation. At 30 min, assembly intermediates with lengths of several hundreds nanometres or more were observed and they showed relatively reduced widths of ~15 nm, suggesting that these filaments were in the course of radial compaction along the filament axis, probably causing reorganization of tetramers within a filament (*15*, *18*, *19*). Finally, at 1h, mature IFs with a length of several micrometres and a width of 14 ± 1 nm were observed (Fig. 3c).

Vim[F14S] performed filament elongation in a time-table similar to that of wild-type vimentin, and finally gave fully elongated (i.e. several micrometers long) mature IFs with a width of 14 ± 1 nm at 1 h (Fig. 3h–j). Thus, although Vim[F14S] formed relatively thick ULFs with a width of ~19 nm at 150 mM NaCl (Fig. 2d), the mutant protein finally gave IFs with almost the same width with that of wild-type vimentin IFs, indicating that striking radial compaction had occurred for the mutant protein during filament elongation (Fig. 3h–j).

Unexpectedly, Vim[Y10N] and Vim[Y10N, F14S] showed extremely rapid filament elongation compared

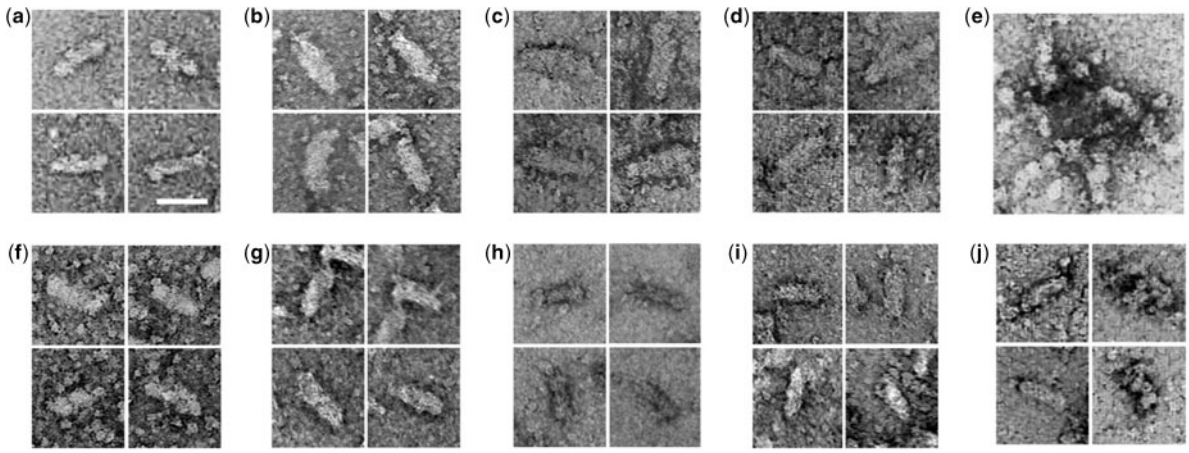

Fig. 2. **ULFs observed by electron microscopy at 2 s after initiation of assembly.** Wild-type vimentin (a and f), Vim[Y10N] (b and g), Vim[Y10N, F14S] (c and h), Vim[F14S] (d and i), and Vim[R11S, R12S] (e and j) were assembled at the concentration of 0.2 mg/ml in an assembly buffer of 20 mM imidazole–HCl pH 7.2, 150 mM NaCl (a–e) or 50 mM NaCl (f–j), 2 mM β-mercaptoethanol at 37°C. At 2 s, assembly reaction was stopped by addition of an equal volume of the assembly buffer containing 0.2% glutaraldehyde, and each sample was served for electron microscopic analysis after negative staining. At 150 mM NaCl the mutant proteins except Vim[R11S, R12S] formed relatively larger ULFs than those of wild-type vimentin, whereas at 50 mM NaCl ULFs of the mutant proteins were about as large as those of wild-type vimentin. Vim[R11S, R12S] formed ULF-like structures besides aggregates at 50 mM NaCl. The scale bar represents 50 nm.

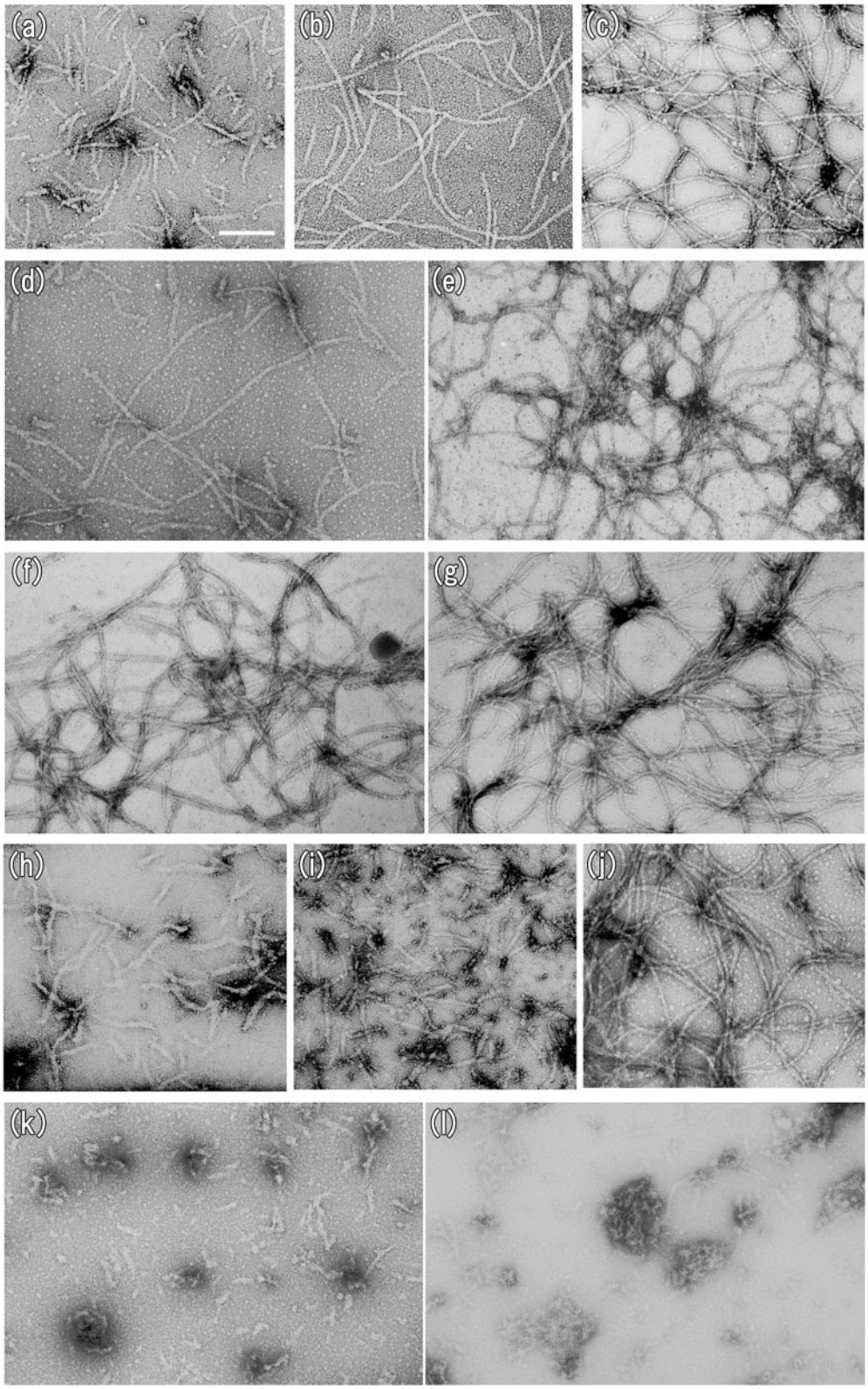

Fig. 3. **Time-dependent assembly of wild-type vimentin (a–c), Vim[Y10N] (d and e), Vim[Y10N, F14S] (f and g), Vim[F14S] (h–j), and Vim[R11S, R12S] (k and l) as observed by electron microscopy after negative staining.** Filament assembly was carried out in 20 mM imidazole–HCl pH 7.2, 150 mM NaCl, 2 mM β-mercaptoethanol at 37°C, and stopped by addition of an equal volume of the assembly buffer containing 0.2% glutaraldehyde after 2.5 min (a, d, f, h and k), 5 min (e, g and l), 10 min (b and i) and 1 h (c and j). Vim[Y10N, F14S] and Vim[Y10N] formed fully elongated IFs within only 2.5 min (f) and 5 min (g), respectively, and their IFs tended to intertwine each other. The scale bar represents 200 nm.

to wild-type vimentin, and formed fully elongated IFs within only 5 min (Fig. 3e) and 2.5 min (Fig. 3f), respectively. Thus, substitution of the aromatic residues, especially Tyr-10, significantly promoted the filament elongation reaction. Substitution of Phe-14 in addition to that of Tyr-10 seemed to have an additive effect in increasing the filament elongation rate, although single substitution of Phe-14 did not show such a prominent effect on filament elongation (Fig. 3h–j). During the rapid filament elongation, drastic radial compaction also occurred, from the widths of ULFs (23 ± 3 nm for Vim[Y10N] and 23 ± 4 nm for Vim[Y10N, F14S]) (Fig. 2b and c), to the widths of IFs (14 ± 1 nm for Vim[Y10N] and 14 ± 1 nm for Vim[Y10N, F14S]) (Fig. 3e and f). Furthermore, IFs of the mutant proteins, especially Vim[Y10N, F14S], tended to intertwine each other and formed bundles in parts of the specimens (Fig. 3e and g). Since the intertwinement and bundle formation were not observed for their ULFs (Fig. 2b and c), these events seemed to occur after the filaments elongated over several hundreds nanometers or more. Further incubation (~1 h) of the assembly mixtures of the mutant proteins led to gradual increase of bundles (data not shown).

Filament elongation of all the proteins apparently slowed down at 50 mM NaCl (Fig. 4), although use of 100 mM NaCl showed subtle effects on the rates of filament elongation (data not shown). Vim[Y10N, F14S] formed fully elongated IFs with a width of 14 ± 1 nm at 10 min (Fig. 4g). Vim[Y10N] afforded IFs with a width of 15 ± 1 nm at 30 min (Fig. 4e). Vim[F14S] as well as wild-type vimentin gave mainly assembly-intermediates with lengths of several hundreds nanometres and width of approximately 15 nm at 1 h (Fig. 4c and l), and did not form fully elongated IFs even at 2 h (data not shown).

Interestingly, Vim[Y10N, F14S] and Vim[Y10N] did not show notable intertwinements of IFs at 50 mM NaCl (Fig. 4d–i). Further incubation (~1 h) did not cause bundle formation (data not shown). Thus, intertwinements and bundle formation of the two mutant proteins depended on the salt concentration. To form normal IFs without intertwinements, the optimal salt concentration for Vim[Y10N, F14S] and Vim[Y10N] appeared to be 50 mM, apparently lower than that (150 mM) for wild-type vimentin. At 20 mM NaCl, however, Vim[Y10N, F14S] and Vim [Y10N] formed only assembly-intermediates with lengths less than ~500 nm and did not form fully elongated mature IFs (data not shown).

Vim[R11S, R12S] gave mainly aggregates at 50–150 mM NaCl (Figs 3k and l, 4m–o), as expected from the previous reports (*21*, *26*, *29*). Sometime short filaments with irregular surfaces were also observed at 50 mM NaCl (Fig. 4m–o). These structures might be formed by annealing of the ULF-like structures observed at 2 s at 50 mM NaCl (Fig. 2j, left side). Thus, the incompetence of this mutant protein to form normal ULFs at the beginning of assembly reaction (Fig. 2e and j) resulted in failure of fully elongated mature IFs. Again, Arg-11 and Arg-12 are critically involved in ULF formation, and substitution of these residues interferes with ULF formation and following filament elongation. In contrast, Tyr-10 and Phe-14 appeared to control intermolecular interactions involved in both ULF formation and filament elongation, depending upon ionic strength employed in the assembly reaction.

Viscosity Measurements—To demonstrate the assembly kinetics, viscosities of the assembly reaction mixtures were measured at each time-point, using an Ostwald-type glass capillary viscometer (*26*, *33*). Assembly reaction was initiated by addition of the soluble proteins to the concentrated assembly buffer and rapid mixing at 30°C. Then, each sample was immediately introduced into the viscometer that was retained at 30°C in advance, and viscosity was measured at regular, specified intervals. Protein concentration was adjusted at 0.3 mg/ml, close to the concentration employed in the electron microscopic analysis.

At 150 mM NaCl, Vim[F14S] as well as wild-type vimentin gave half-maximal viscosity at ~20 min, then reached a plateau at 40–60 min (Fig. 5a), consistent with the observation in electron microscopy that they formed fully elongated filaments at 1 h (Fig. 3c and j). In contrast, Vim[Y10N, F14S] and Vim[Y10N] showed a drastic increase in viscosity immediately after initiation of the assembly reaction (Fig. 5a), reflecting rapid filament elongation as observed in electron microscopy (Fig. 3e and f). Their viscosities increased up to ~2-fold higher values than that of wild-type vimentin. The very high viscosities observed for Vim[Y10N, F14S] at 5 min and for Vim[Y10N] at 20 min are probably due to aggregation of their filaments during viscosity measurements. In fact, after reaching the maximal viscosity values, insoluble aggregates were observed in the reaction mixtures and they interfered with a subsequent measurement.

As the salt concentration was reduced to 100 mM (data not shown) or 50 mM (Fig. 5b), each protein exhibited a lower kinetics in viscosity measurement. At 50 mM NaCl, Vim[Y10N] and Vim[Y10N, F14S] (Fig. 5b) gave curves similar to those observed for Vim[F14S] and wild-type vimentin at 150 mM NaCl (Fig. 5a). In fact, as shown in electron microscopy, Vim[Y10N, F14S] and Vim[Y10N] formed normally elongated IFs at 30 min and 1 h, respectively, at 50 mM NaCl (Fig. 4f and h). In contrast, Vim [F14S] as well as wild-type vimentin showed only a small increase in viscosity at 50 mM NaCl (Fig. 5b). This was consistent with the electron microscopic observation in that Vim[F14S] and wild-type vimentin afforded mainly assembly intermediates at 50 mM NaCl (Fig. 4c and l).

Initial rate in the increase of viscosity of each protein (Fig. 5c) suggest that ULFs of Vim[Y10N] and Vim[Y10N, F14S] possess ~3- and 6-hold higher potentials, respectively, to anneal to each other than do ULFs of wild-type vimentin. Thus, the results of viscosity measurements correlated well with the morphological data obtained by electron microscopy, and confirmed that Vim[Y10N, F14S] and Vim[Y10N] assemble into IFs with significantly higher efficiencies than those of Vim[F14S] and wild-type vimentin.

DISCUSSION

Under a standard IF assembly condition containing 150 mM NaCl, Vim[Y10N, F14S] and Vim[Y10N] formed relatively thick ULFs and then showed very fast longitudinal annealing of ULFs. The two vimentin mutants formed fully elongated IFs within only 5 min, although they showed a tendency to intertwine each other and formed filament bundles in parts of the specimens. To form

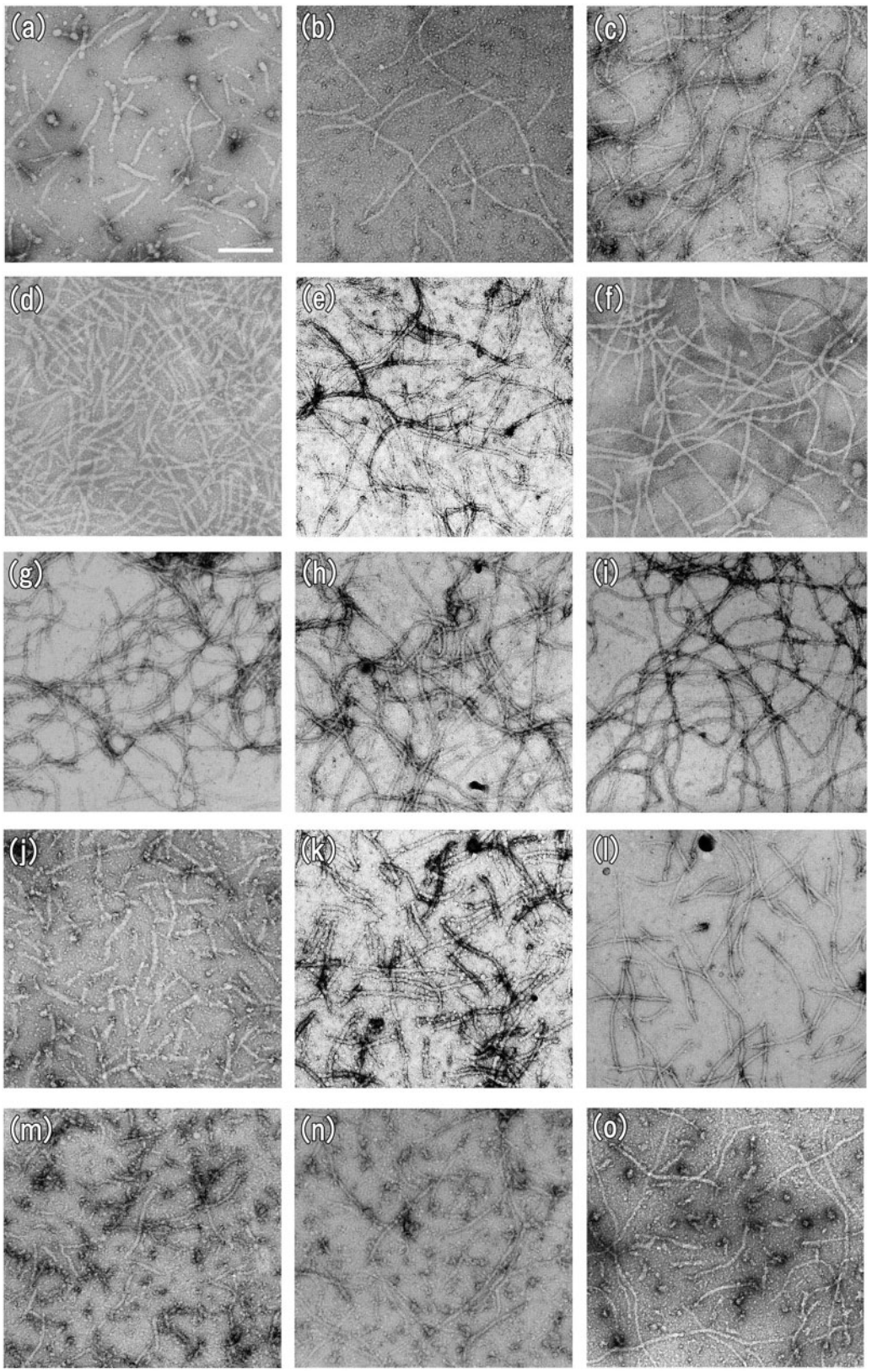

Fig. 4. **Time-dependent assembly of wild-type vimentin (a–c), Vim[Y10N] (d–f), Vim[Y10N, F14S] (g–i), Vim[F14S] (j–l) and Vim[R11S, R12S] (m–o) as observed by electron microscopy after negative staining.** Filament assembly was carried out in 20 mM imidazole–HCl pH 7.2, 50 mM NaCl, 2 mM β-mercaptoethanol at 37°C, and stopped by addition of an equal volume of the assembly buffer containing 0.2% glutaraldehyde after 10 min (a, d, g, j and m), 30 min (b, e, h, k and n) and 1 h (c, f, i, l and o). The scale bar represents 200 nm.

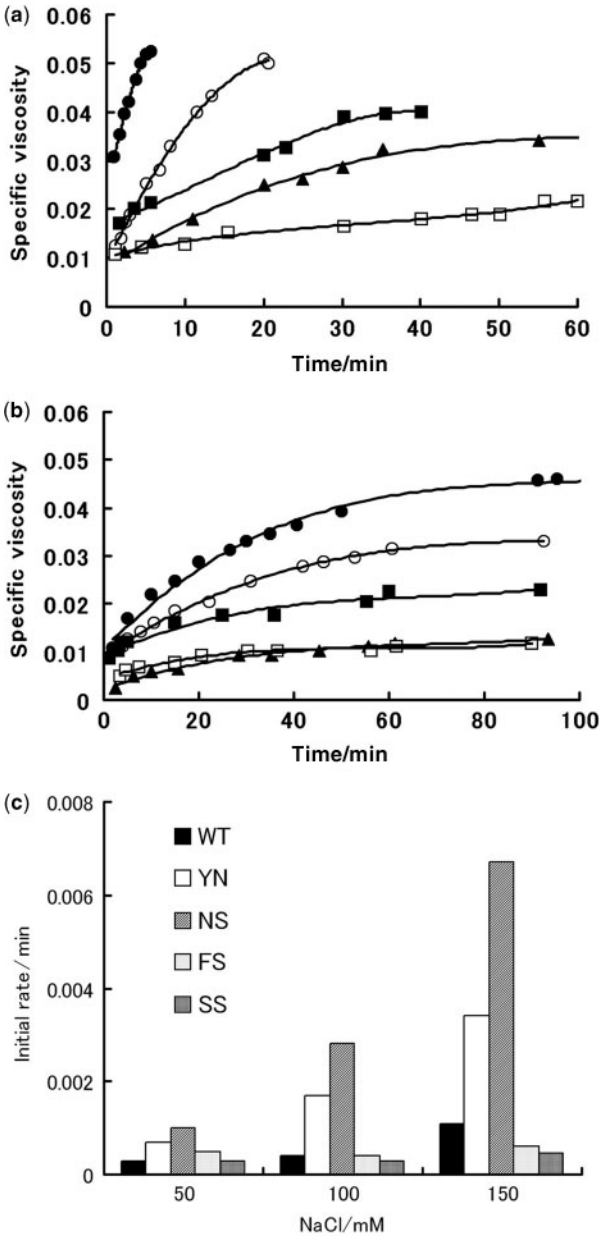

Fig. 5. **Viscosity measurements of wild-type vimentin (filled triangles), Vim[Y10N] (open circles), Vim[Y10N, F14S] (filled circles), Vim[F14S] (filled squares) and Vim[R11S, R12S] (open squares), in the assembly buffer pH 7.2 containing 150 mM NaCl (a) or 50 mM NaCl (b).** Each protein (0.3 mg/ml) was assembled at 30°C, and viscosity was measured, as described under MATERIALS AND METHODS section. The curves were fitted by cubic equations. (c) Initial rate in the increase of viscosity was estimated by differential of the equation at time zero second. WT, wild-type vimentin; YN, Vim[Y10N]; NS, Vim[Y10N, F14S]; FS, Vim[F14S]; SS, Vim[R11S, R12S].

normal IFs within 1 h, 50 mM NaCl was observed to be optimal for the mutant proteins. These results suggest that Tyr-10 and Phe-14 have a role to regulate the intermolecular interactions involved in vimentin IF assembly and suppress unfavourable aggregation of IFs at physiological ionic strength.

Individual IF proteins strikingly differ with respect to their IF assembly conditions *in vitro* (*1*, *4*, *5*, *16*), although biological significance is unknown. Our results call attention to the aromatic residues, Tyr-10 and Phe-14, in the near-amino terminal motif of vimentin as a structural element that determines an optimal ionic strength for IF assembly *in vitro*, although other parts of the head domain sequences might be also important. Type III IF proteins such as vimentin and desmin containing a sequence of -Tyr-Arg-Arg-X-Phe-, and type IV neurofilament protein-L containing a sequence of -Tyr-Lys-Arg-Arg-Phe-, need a relatively high concentration (100–160 mM) of NaCl or KCl to form fully elongated mature IFs (*14*, *16*, *19*, *26*, *28*, *29*, *32*, *34–37*). Another type III protein of glial fibrillary acidic protein containing a sequence of -Ala/Thr-Arg-Arg-Ser-Tyr- prefers a relatively low concentration (50–100 mM) of NaCl or KCl (*38*, *39*). On the other hand, type I and type II cytokeratins co-polymerize into IFs at 0–50 mM NaCl (*13*, *16*, *17*, *40*). The cytokeratins do not have a definite motif composed of arginine and aromatic residues, although an average of ~6 arginines and ~11 aromatic residues exist in the head domain. Employment of a higher concentration of NaCl (>50 mM) results in formation of aggregates. It was also reported that, cytokeratins 8 and 18 perform longitudinal filament growth very rapidly, almost simultaneously with ULF formation at 50 mM NaCl (*17*). In this study, substitution of Tyr-10 and Phe-14 of vimentin strikingly accelerated the longitudinal filament elongation and reduced the optimal salt concentration close to that for the cytokeratins.

Previously, Herrmann *et al*. have reported that simultaneous substitution of the two aromatic residues and isoleucine in the near-amino-terminal motif (-Tyr-Arg-Arg-Ile-Phe-) of *Xenopus* vimentin with three serine residues resulted in the formation of dense aggregates at 160 mM NaCl (*26*). Since assembly-intermediates of the mutant protein were not analyzed by the authors, it is unknown whether the mutant protein forms ULFs and undergoes longitudinal annealing of ULFs before forming the aggregates. The isoleucine residue with the hydrophobic bulky side chain might be also important for IF assembly of *Xenopus* vimentin.

In this study, substitution of Tyr-10 and Phe-14 of vimentin appeared to enhance intermolecular interactions involved in ULF formation and filament elongation. In ULF formation, vimentin tetramers in the A_{11} alignment and the A_{22} alignment associate laterally (*9–12*, *18*). In the following filament elongation, ULFs anneal longitudinally each other at their both ends (*15–17*, *19*). Although structures of the molecular interfaces on the assembly intermediates are unknown, the interfaces are likely formed by cooperative interaction between the head domain and a certain part of the rod domain, because a vimentin mutant lacking the head domain does not form ULF nor IFs (*5*, *15*, *23–25*) and the vimentin head domain has been shown to interact with the rod domain (*26*, *27*, *29*, *30*, *37*). In the interaction between the head domain and the rod domain, the near-amino terminal motif of vimentin has been assigned as a critical structural element (*5*, *26*, *27*, *29*). Especially, the two adjacent arginine residues, Arg-11 and Arg-12, in the motif are expected to play an essential role in the

interaction with the rod domain, because synthetic peptides representing the near-amino terminal motif of vimentin lose an activity interfering with IF assembly of wild-type vimentin, by substituting the arginine residues in the peptides with other neutral amino acids (*5*, *27*).

We presume that Tyr-10 and Phe-14 have a role to control functions of Arg-11 and Arg-12 in the interaction with the rod domain, as follows. The cationic charges of the arginine residues can interact with anionic charges of acidic residues that are abundant in the rod domain. However, simple salt bridge formation with the rod domain does not seem to be responsible for vimentin IF assembly, since this process is favored at the elevated ionic strength (*14*, *26*, *28*, *29*, *37*). It is well known that the multi-functional behaviour of arginine contributes making up specific conformation of proteins and protein–ligand complexes. The guanidinium group has a high capacity to donate hydrogen bonds. The methylene groups can contribute favorably to the hydrophobic effect. Furthermore, the cationic side chain is potentially beneficial to form cation-π interactions with aromatic side chains having high electron density (*41–43*). The cation-π interactions are calculated to be more stabilizing than salt-bridges, and are not strongly attenuated in water. It is conceivable that Tyr-10 and Phe-14 form cation-π interactions with Arg-11 and Arg-12. Simultaneously, the arginines in the motif might form salt-bridges or hydrogen bonds with a specific binding site in the rod domain, since it has been observed that more than half of arginines involved in the cation-π interaction are involved in salt-bridges or hydrogen bonds with an interacting partner surface (*43*). In such a case, the cation-π interaction and the salt-bridges are augmented each other (*43*). The putative cation-π interaction within the near amino-terminal motif might contribute to targeting the side chains of Arg-11 and Arg-12 to a specific binding site in the rod domain (*41*, *43*). Our observation that substitution of Tyr-10 gave a more significant effect on IF assembly than did substitution at Phe-14 suggest that Tyr-10 is primarily involved in controlling the functions of the neighbouring arginines. This is in good agreement with the previous report that arginine–tyrosine pairs are most abundant in the cation-π interactions (*43*).

According to the above assumption, substitution of Tyr-10 and Phe-14 extinguishes the cation-π interaction within the motif. Alternatively, the arginines in the motif can form new cation-π interactions with aromatic residues located in the rod domain, in addition to the salt-bridges or hydrogen bonds so far formed. The new cation-π interactions would enhance the interaction with the rod domain. Such alterations in the interaction between the near-amino terminal motif and the rod domain might change the structures of the molecular interfaces on vimentin tetramers and ULFs, then might lead to enhancement of salt-stable intermolecular interactions in ULF formation and filament elongation, as observed here. To prove this hypothesis, it is urgent to identify the specific binding site of the near-amino terminal motif of vimentin. While the rod domain is throughout wealthy with acidic residues, the aromatic residues are relatively abundant in helices 1a and 2b rather than helices 1b and 2a. Especially, the conserved N-terminal end of helix 1a and the conserved C-terminal end of helix 2b, which have been shown to be critically involved in IF assembly (*22*, *30*, *37*, *44*), are a candidate for the target site of the near-amino terminal motif.

ACKNOWLEDGEMENTS

We are grateful to Drs Y. Yamaguchi and M. Miyazaki of National Institute of Advanced Industrial Science and Technology, Kyushu (AIST-Kyushu) for pertinent comments and discussions.

CONFLICT OF INTEREST

None declared.

REFERENCES

1. Fuchs, E. and Weber, K (1994) Intermediate filaments: structure, dynamics, function, and disease. *Annu. Rev. Biochem.* **63**, 345–382
2. Inagaki, M., Matsuoka, Y., Tsujimura, K., Ando, S., Tokui, T., Takahashi, T., and Inagaki, N. (1996) Dynamic property of intermediate filaments: regulation by phosphorylation. *BioEssays* **18**, 481–487
3. Goldman, R.D., Chou, Y.-H., Prahlad, V., and Yoon, M. (1999) Intermediate filaments: dynamic processes regulating their assembly, motility, and interactions with other cytoskeletal systems. *FASEB J.* **13**, S261–S265
4. Parry, D.A.D. and Steinert, P.M. (1999) Intermediate filaments: molecular architecture, assembly, dynamics and polymorphism. *Q. Rev. Biophys.* **32**, 99–187
5. Herrmann, H. and Aebi, U. (2004) Intermediate filaments: molecular structure, assembly mechanism, and integration into functionally distinct intracellular scaffolds. *Annu. Rev. Biochem.* **73**, 749–789
6. Parry, D.A.D., Strelkov, S.V., Burkhard, P., Aebi, U., and Herrmann, H. (2007) Towards a molecular description of intermediate filament structure and assembly. *Exp. Cell Res.* **313**, 2204–2216
7. Magin, T.M., Reichelt, J., and Hatzfeld, M. (2004) Emerging function: diseases and animal models reshape our view of the cytoskeleton. *Exp. Cell Res.* **301**, 91–102
8. Hess, M., Magin, T.M., and Weber, K. (2001) Genes for intermediate filament proteins and the draft sequence of the human genome: novel keratin genes and a surprisingly high number of pseudogenes related to keratin genes 8 and 18. *J. Cell Sci.* **114**, 2569–2575
9. Geisler, N., Schünemann, J., and Weber, K. (1992) Chemical cross-linking indicates a staggered and antiparallel protofilament of desmin intermediate filaments and characterizes one higher-level complex between protofilaments. *Eur. J. Biochem.* **206**, 841–852
10. Steinert, P.M., Marekov, L.N., and Parry, D.A. (1993) Diversity of intermediate filament structure. Evidence that the alignment of coiled-coil molecules in vimentin is different from that in keratin intermediate filaments. *J. Biol. Chem.* **268**, 24916–24925
11. Rogers, K.R., Herrmann, H., and Franke, W.W. (1996) Characterization of disulfide crosslink formation of human vimentin at the dimer, tetramer, and intermediate filament levels. *J. Struct. Biol.* **117**, 55–69
12. Hess, J.F., Budamagunta, M.S., Voss, J.C., and FitzGerald, P.G. (2004) Structural characterization of human vimentin rod 1 and the sequencing of assembly steps in intermediate filament formation *in vitro* using site-directed spin labeling and electron paramagnetic resonance. *J. Biol. Chem.* **279**, 44841–44846
13. Wu, C., Bryan, J.T., Morasso, M.I., Jang, S.-I., Lee, J.-H., Yang, J.-M., Marekov, L. N., Parry, D.A.D., and Steinert, P.M.

(2000) Coiled-coil trigger motifs in the 1B and 2B rod domain segments are required for the stability of keratin intermediate filaments. *Mol. Biol. Cell* **11**, 3539–3558
14. Ip, W., Hartzer, M.K., Pang, Y.-Y. S., and Robson, R.M. (1985) Assembly of vimentin *in vitro* and its implications concerning the structure of intermediate filaments. *J. Mol. Biol.* **183**, 365–375
15. Herrmann, H., Häner, M., Brettel, M., Müller, S.A., Goldie, K.N., Fedtke, B., Lustig, A., Franke, W.W., and Aebi, U. (1996) Structure and assembly properties of the intermediate filament protein vimentin: the role of its head, rod and tail domains. *J. Mol. Biol.* **264**, 933–953
16. Herrmann, H., Häner, M., Brettel, M., Ku, N.-O., and Aebi, U. (1999) Characterization of distinct early assembly units of different intermediate filament proteins. *J. Mol. Biol.* **286**, 1403–1420
17. Herrmann, H., Wedig, T., Porter, R.M., Lane, E.B., and Aebi, U. (2002) Characterization of early assembly intermediates of recombinant human keratins. *J. Struct. Biol.* **137**, 82–96
18. Mücke, N., Wedig, T., Bürer, A., Marekov, L.N., Steinert, P.M., Langowski, J., Aebi, U., and Herrmann, H. (2004) Molecular and biophysical characterization of assembly-starter units of human vimentin. *J. Mol. Biol.* **340**, 97–114
19. Ando, S., Nakao, K., Gohara, R., Takasaki, Y., Suehiro, K., and Oishi, Y. (2004) Morphological analysis of glutaraldehyde-fixed vimentin intermediate filaments and assembly-intermediates by atomic force microscopy. *Biochim. Biophys. Acta* **1702**, 53–65
20. Hatzfeld, M. and Weber, K. (1991) Modulation of keratin intermediate filament assembly by single amino acid exchanges in the consensus sequence at the C-terminal end of the rod domain. *J. Cell Sci.* **99**, 351–362
21. Raats, J.M.H., Gerards, W.L.H., Schreuder, M.I., Grund, C., Henderik, J.B.J., Hendriks, I.L.A.M., Ramaekers, F.C.S., and Bloemendal, H. (1992) Biochemical and structural aspects of transiently and stably expressed mutant desmin in vimentin-free and vimentin-containing cells. *Eur. J. Cell Biol.* **58**, 108–127
22. Herrmann, H., Strelkov, S.V., Feja, B., Rogers, K.R., Brettel, M., Lustig, A., Häner, M., Parry, D.A.D., Steinert, P.M., Burkhard, P., and Aebi, U. (2000) The intermediate filament protein consensus motif of helix 2B: its atomic structure and contribution to assembly, *J. Mol. Biol.* **298**, 817–832
23. Traub, P. and Vorgias, C. E. (1983) Involvement of the N-terminal polypeptide of vimentin in the formation of intermediate filaments. *J. Cell Sci.* **63**, 43–67
24. Coulombe, P.A., Chan, Y.M., Albers, K., and Fuch, E. (1990) Deletions in epidermal keratins leading to alterations in filament organization *in vivo* and in intermediate filament assembly *in vitro*. *J. Cell Biol.* **111**, 3049–3064
25. Raats, J.M.H., Pieper, F.R., Vree Egberts, W.T.M., Verrijp, K.N., Ramaekers, F.C.S., and Bloemendal, H. (1990) Assembly of amino-terminally deleted desmin in vimentin-free cells. *J. Cell Biol.* **111**, 1971–1985
26. Herrmann, H., Hofmann, I., and Franke, W.W. (1992) Identification of a nonapeptide motif in the vimentin head domain involved in intermediate filament assembly. *J. Mol. Biol.* **223**, 637–650
27. Hofmann, I. and Herrmann, H. (1992) Interference in vimentin assembly *in vitro* by synthetic peptides derived from the vimentin head domain. *J. Cell Sci.* **101**, 687–700
28. Hatzfeld, M., Dodemont, H., and Weber, K. (1992) Truncation of recombinant vimentin by ompT, identification of a short motif in the head domain necessary for assembly of type III intermediate filament proteins. *FEBS Lett.* **302**, 239–242
29. Beuttenmüller, M., Chen, M., Janetzko, A., Kühn, S., and Traub, P. (1994) Structural elements of the amino-terminal head domain of vimentin essential for intermediate filament formation *in vivo* and *in vitro*. *Exp. Cell Res.* **213**, 128–142
30. Gohara, R., Tang, D., Inada, H., Inagaki, M., Takasaki, Y., and Ando, S. (2001) Phosphorylation of vimentin head domain inhibits interaction with the carboxyl-terminal end of α-helical rod domain studied by surface plasmon resonance measurements. *FEBS Lett.* **489**, 182–186
31. Bradford, M.M. (1976) A rapid and sensitive method for the quantitation of microgram quantities of protein utilizing the principle of protein-dye binding. *Anal. Biochem.* **72**, 248–254
32. Heins, S., Wong, P.C., Müller, S., Goldie, K., Cleveland, D.W., and Aebi, U. (1993) The rod domain of NF-L determines neurofilament architecture, whereas the end domains specify filament assembly and network formation. *J. Cell Biol.* **123**, 1517–1533
33. Hofmann, I. (1998) Measuring the assembly kinetics and binding properties of intermediate filament proteins. *Subcell. Biochem.* **31**, 363–380
34. Huiatt, T.W., Robson, R.M., Arakawa, N., and Stromer, M.H. (1980) Desmin from avian muscle: purification and partial characterization. *J. Biol. Chem.* **255**, 6981–6989
35. Inagaki, M., Gonda, Y., Matsuyama, M., Nishizawa, K., Nishi, Y., and Sato, C. (1988) Intermediate filament reconstitution *in vitro*: the role of phosphorylation on the assembly-disassembly of desmin. *J. Biol. Chem.* **263**, 5970–5978
36. Hisanaga, S. and Hirokawa, N. (1990) Molecular architecture of the neurofilament II. Reassembly process of neurofilament L protein *in vitro*. *J. Mol. Biol.* **211**, 871–882
37. Traub, P., Scherbarth, A., Wiegers, W., and Shoeman, R.L. (1992) Salt-stable interaction of the amino-terminal head region of vimentin with the α-helical rod domain of cytoplasmic intermediate filament proteins and its relevance to protofilament structure and filament formation and stability. *J. Cell Sci.* **101**, 363–381
38. Inagaki, M., Gonda, Y., Nishizawa, K., Kitamura, S., Sato, C., Ando, S., Tanabe, K., Kikuchi, K., Tsuiki, S., and Nishi, Y. (1990) Phosphorylation sites linked to glial filament disassembly *in vitro* locate in a non-α-helical head domain. *J. Biol. Chem.* **265**, 4722–4729
39. Ralton, J.E., Lu, X., Hutcheson, A.M., and Quinlan, R.A. (1994) Identification of two N-terminal non-alpha-helical domain motifs important in the assembly of glial fibrillary acidic protein. *J. Cell Sci.* **107**, 1935–1948
40. Yano, T., Tokui, T., Nishi, Y., Nishizawa, K., Shibata, M., Kikuchi, K., Tsuiki, S., Yamauchi, T., and Inagaki, M. (1991) Phosphorylation of keratin intermediate filaments by protein kinase C, by calmodulin-dependent protein kinase and by cAMP-dependent protein kinase. *Eur. J. Biochem.* **197**, 281–290
41. Gallivan, J.P. and Dougherty, D.A. (1999) Cation-π interactions in structural biology. *Proc. Natl Acad. Sci. USA* **96**, 9459–9464
42. Burghardt, T.P., Juranić, N., Macura, S., and Ajtai, K. (2002) Cation-π interaction in a folded polypeptide. *Biopolymers* **63**, 261–272
43. Crowley, P.B. and Golovin, A. (2005) Cation-π interactions in protein-protein interactions. *Proteins* **59**, 231–239
44. Strelkov, S.V., Herrmann, H., Geisler, N., Wedig, T., Zimbelmann, R., Aebi, U., and Burkhard, P. (2002) Conserved segments 1A and 2B of the intermediate filament dimer: their atomic structures and role in filament assembly. *EMBO J.* **21**, 1255–1266